

**The following resources related to this article are available online at [www.sciencemag.org](http://www.sciencemag.org) (this information is current as of December 24, 2009):**

**Updated information and services**, including high-resolution figures, can be found in the online version of this article at:

<http://www.sciencemag.org/cgi/content/full/310/5756/1938>

**Supporting Online Material** can be found at:

<http://www.sciencemag.org/cgi/content/full/310/5756/1938/DC1>

A list of selected additional articles on the Science Web sites **related to this article** can be found at:

<http://www.sciencemag.org/cgi/content/full/310/5756/1938#related-content>

This article **cites 14 articles**, 2 of which can be accessed for free:

<http://www.sciencemag.org/cgi/content/full/310/5756/1938#otherarticles>

This article has been **cited by** 10 article(s) on the ISI Web of Science.

This article appears in the following **subject collections**:

Chemistry

<http://www.sciencemag.org/cgi/collection/chemistry>

Information about obtaining **reprints** of this article or about obtaining **permission to reproduce this article** in whole or in part can be found at:

<http://www.sciencemag.org/about/permissions.dtl>

- time span simulated (fig. S6 and table S8). These results, combined with the lack of resolution within superclades of the metazoan tree, argue against models of metazoan radiation in which the temporal window of diversification is much larger (48).
39. J. A. Clack, *Gaining Ground: the Origin and Evolution of Tetrapods* (Indiana Univ. Press, Bloomington, IN, 2002).
40. N. Takezaki, F. Figueroa, Z. Zaleska-Rutczynska, N. Takahata, J. Klein, *Mol. Biol. Evol.* **21**, 1512 (2004).
41. Y. I. Wolf, I. B. Rogozin, E. V. Koonin, *Genome Res.* **14**, 29 (2004).
42. J. E. Blair, K. Ikeo, T. Gojobori, S. B. Hedges, *BMC Evol. Biol.* **2**, 7 (2002).

43. H. Philippe, N. Lartillot, H. Brinkmann, *Mol. Biol. Evol.* **22**, 1246 (2005).
44. S. L. Baldauf, J. D. Palmer, *Proc. Natl. Acad. Sci. U.S.A.* **90**, 11558 (1993).
45. J. L. Boore, D. Lavrov, W. M. Brown, *Nature* **393**, 667 (1998).
46. A. Rokas, P. W. H. Holland, *Trends Ecol. Evol.* **15**, 454 (2000).
47. A goodness-of-fit test using parametric bootstrapping (15) showed that even the best-fit model of sequence evolution does not adequately describe the evolution of the sequence data from these 32 fungal and metazoan taxa (fig. S8).

48. G. A. Wray, J. S. Levinton, L. H. Shapiro, *Science* **274**, 568 (1996).
49. We thank D. Arendt for providing RNA for *Platynereis dumerilii*; C. Ané for providing the modified version of the Seq-Gen simulation software with an implementation of a covarion model; and B. Prud'homme, B. Williams, and T. Rokas for comments on the manuscript. A.R. was funded by a Human Frontier Science Program Long-Term Fellowship. This work was funded by the Howard Hughes Medical Institute.

29 June 2005; accepted 4 November 2005  
10.1126/science.1116759

# REPORTS

## Separation and Conversion Dynamics of Four Nuclear Spin Isomers of Ethylene

Zhen-Dong Sun,\* Kojiro Takagi, Fusakazu Matsushima

Molecules with three or more nuclei of nonzero spin exist as discrete spin isomers whose interconversion in the gas phase is generally considered improbable. We have studied the interconversion process in ethylene by creating a sample depleted in the  $B_{2u}$  nuclear spin isomer. The separation was achieved through spatial drift of this isomer induced by resonant absorption of narrow-band infrared light. Evolution of the depleted sample revealed conversion between  $B_{2u}$  and  $B_{3u}$  isomers at a rate linearly proportional to pressure, with a rate constant of  $5.5 (\pm 0.8) \times 10^{-4} \text{ s}^{-1} \text{ torr}^{-1}$ . However, almost no change was observed in the  $A_g$  isomer populations. The results suggest a spin conversion mechanism in  $\text{C}_2\text{H}_4$  via quantum relaxation within the same inversion symmetry.

Nuclear spin isomers and their stability are fundamental concepts in quantum mechanics (1). In accordance with Pauli's principle, all molecules possessing identical nuclei with nonzero spin have distinct nuclear spin isomers (1). However, despite continuous study following the first separation and conversion of *ortho*- and *para*- $\text{H}_2$  in 1929 (2), the interconversion dynamics of three or more isomers in larger polyatomic molecules remain poorly understood. In astronomy and astrophysics, the abundance ratios of nuclear spin isomers in the interstellar medium (ISM) are key parameters in probing the formation conditions in the past and anticipating subsequent processes in the future evolution of planetary materials and protostellar environments (3–5). It is widely assumed that the conversion probabilities among nuclear spin isomers for the various molecules in the ISM are zero, even over time spans of millions of years. However, this is not necessarily the case (6–10).

Department of Physics, University of Toyama, Toyama 930-8555, Japan.

\*To whom correspondence should be addressed.  
E-mail: zdsun@unbsj.ca

To date, separation and conversion of nuclear spin isomers have been successfully studied for only a small number of polyatomic molecules:  $\text{CH}_3\text{F}$  (6, 7),  $^{13}\text{C}^{12}\text{CH}_4$  (8),  $\text{H}_2\text{CO}$  (9), and  $\text{H}_2\text{O}$  (11). Among the separation methods (6, 9, 11), the light-induced drift (LID) (12) technique is one of the more powerful and sensitive tools. The principle of LID can be briefly described as follows: Let a powerful laser pass through a closed cell containing a low-pressure gas mixture of a laser-absorbing species and a nonabsorbing buffer gas. When the laser frequency is tuned to, for example, the red wing of the spectral Doppler absorption profile, a certain velocity class of absorbing molecules moving toward the laser will be excited as a result of the Doppler effect. Because the excited molecules usually have a larger cross section than the ground-state molecules, their mean free path will be smaller than that of the ground-state molecules. This produces a drift of the absorbing species moving in the direction of the laser beam with respect to the buffer gas and results in a concentration difference between the two ends of the closed cell. So far, however, insights from LID

studies have been limited to molecules with only *ortho* and *para* isomers (gaseous  $\text{CH}_3\text{F}$  and  $^{13}\text{C}^{12}\text{CH}_4$ ). For a molecule with more than two nuclear spin isomers, such as the four isomers ( $A_g$ ,  $B_{1g}$ ,  $B_{2u}$ , and  $B_{3u}$ ) of  $^{12}\text{C}_2\text{H}_4$  ethylene, the possibility of interconversion remains experimentally unexplored. To address this question, we have assembled a spectrometer, following the design of Nagels *et al.* (7), to separate and monitor potential interconversion among the  $^{12}\text{C}_2\text{H}_4$  nuclear spin isomers.

Ethylene has a simple structure and a point group ( $D_{2h}$ ) of high symmetry. There are two zero-spin  $^{12}\text{C}$  nuclei and four hydrogens with active spins of  $1/2$ . However, unlike *ortho/para* hydrogen, one cannot visualize the isomers by flipping the spin of individual nuclei. The symmetry characteristics of the four nuclear spin isomers of  $\text{C}_2\text{H}_4$  are listed in Table 1 (13). Here the coordinate system and group theoretical definitions are the same as those given in the textbook by Herzberg (14) and that by Landau and Lifshitz (1), the  $x$ - $y$  plane with the  $x$  axis parallel to the  $\text{C}=\text{C}$  double bond is the molecular plane, and the  $z$  axis is vertical to it. The four nuclear spin species correspond to different classes of  $J_{K_a K_c}$  rotational levels in the ground rovibrational state, where  $J$ ,  $K_a$ , and  $K_c$  refer to the quantum numbers for rotational angular momentum and its projections along the  $x$  and  $z$  axes, respectively. An energy level of  $\text{C}_2\text{H}_4$  is of even or odd parity with regard to the inversion operation  $E^*$  in  $D_{2h}(M)$  in the molecular symmetry group (10). As the parity is given by  $(-1)^{K_c}$  (15), the subscripts  $g$  or  $u$  in

**Table 1.** Species of nuclear spin isomers (NSI) of  $\text{C}_2\text{H}_4$  (1, 14).  $W$  is the statistical weight,  $I$  is the total spin of four equivalent hydrogen nuclei, and even and odd refer to whether  $K_a$  and  $K_c$  are even or odd integers.

NSI	$W$	$I$	$K_a$	$K_c$
$A_g$	7	2, 0	Even	Even
$B_{1g}$	3	1	Odd	Even
$B_{3u}$	3	1	Even	Odd
$B_{2u}$	3	1	Odd	Odd

**Table 2.** Experimental schemes and determined absorption coefficient  $\beta$  ( $\text{cm}^{-1} \text{ torr}^{-1}$ ), the percentage of enrichment or depletion (negative values) at a pressure of 1 torr for a 3-min separation period, and pressure dependence of conversion rate  $\gamma = k\rho + y$  of  $\text{C}_2\text{H}_4$  at a temperature of

Case and number	Rovibrational transition	NSI	Laser line	$\Delta f$ (MHz)	$\beta$	Enrichment	$k$ ( $10^{-4}$ )	$y$ ( $10^{-4}$ )
Separation	$9_{0,9} \leftarrow 10_{1,9}$	$B_{2u}$	10P44	61				
Probe 1	$9_{0,9} \leftarrow 10_{1,9}$	$B_{2u}$	10P44	61	$0.019 \pm 0.001$	$-2.55 \pm 0.50$	$5.76 \pm 1.12$	$1.02 \pm 1.98$
2	$5_{0,5} \leftarrow 4_{1,3}$	$B_{2u}$	10P10	-100	$0.059 \pm 0.002$	$-3.55 \pm 0.50$	$5.79 \pm 0.59$	$1.59 \pm 1.17$
3	$6_{1,5} \leftarrow 6_{2,5}$	$B_{3u}$	10P26	112	$0.097 \pm 0.003$	$0.91 \pm 0.10$	$5.05 \pm 0.57$	$2.57 \pm 0.83$
4	$4_{3,1} \leftarrow 3_{2,1}$	$B_{3u}$	10R22	102	$0.083 \pm 0.002$	$0.94 \pm 0.10$	$5.41 \pm 0.92$	$2.14 \pm 1.13$
5	$6_{3,4} \leftarrow 5_{2,4}$	$A_g$	10R28	-228	$0.191 \pm 0.001$	$0.76 \pm 0.15$		
Average of cases 1 to 4							$5.5 \pm 0.8$	$1.8 \pm 1.3$

the symmetry representations correspond to even or odd parity of an energy level.

We now report the successful use of LID to deplete the population of the  $B_{2u}$  isomer in a sample of gaseous ethylene, followed by monitoring of the subsequent spin conversions for the return to equilibrium. We measured isomer concentrations by recording the absorption intensities of spectral lines with appropriate  $J$ ,  $K_a$ , and  $K_c$  quantum numbers. Our experimental setup uses two  $\text{CO}_2$  lasers (Edinburgh Instruments PL3 as the separation laser and a home-built laser as the probe) and three glass cells (for separation, test, and reference) (16). We measured the spin conversion rates for  $^{13}\text{CH}_3\text{F}$  with this setup and obtained good agreement with the published results (6, 7).

For the ethylene study, the experimental schemes are shown in Table 2, where the reported results from high-resolution infrared spectroscopy (17) were used to calculate the frequency offsets between the  $\text{C}_2\text{H}_4$  transition frequencies and the  $\text{CO}_2$  laser frequencies. Application of the LID technique for the separation of nuclear spin isomers requires that a molecular transition be near-coincident with a  $\text{CO}_2$  laser line. Here, the 10P44 laser line with a power of 6 W was used. Its frequency was tuned about 20 MHz above the center frequency by adjusting the laser cavity length to set it in the red wing of the  $9_{0,9} \leftarrow 10_{1,9}$  line of the  $\nu_7$  band of ethylene. This frequency selectively excited the  $B_{2u}$  isomer, with the other three isomers acting as a buffer gas. The  $B_{2u}$  molecules drift, by the LID effect, along the direction of the separation laser beam in the separation cell, thereby depleting the  $B_{2u}$  species and enriching the  $A_g$ ,  $B_{1g}$ , and  $B_{3u}$  species at the entrance end of the cell; this direction of drift corresponds to an increase in the collision cross section upon excitation. The nonequilibrium population was then transferred through a valve from the near end of the separation cell to the test cell. For high sensitivity, we measured differential absorption by splitting the probe beam to acquire simultaneous data from the test cell and the reference cell with a population at thermal equilibrium. We determined normalized absorption intensity differences for appropriate probe lines to

300 K, where  $k$ ,  $p$ , and  $y$  are in units of  $\text{s}^{-1} \text{ torr}^{-1}$ , torr, and  $\text{s}^{-1}$ , respectively. Rovibrational transition is from the ground state to the  $\nu_7 = 1$  state. Frequency offset  $\Delta f$  denotes the  $\text{C}_2\text{H}_4$  transition frequency minus the  $\text{CO}_2$  laser frequency.

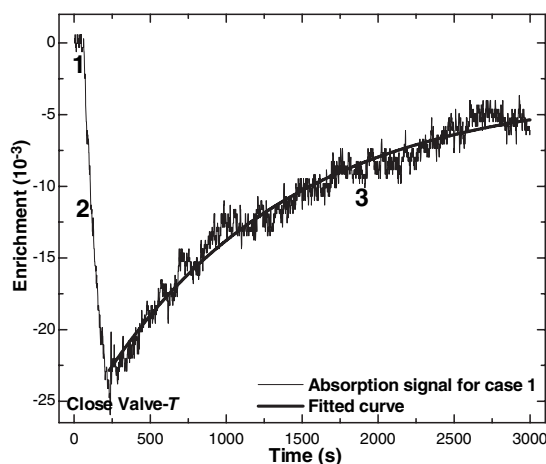


**Fig. 1.** Recorded differential absorption signal at lock-in time constant of 0.3 s using the 10P44 probe  $\text{CO}_2$  laser line at a pressure of 1.44 torr. The trace in the first period is the zero-difference baseline. The trace in the second period shows depletion of 2.46% ( $\pm 0.20\%$ ) for 3 min, and the trace in the third period shows the conversion after the valve is closed.

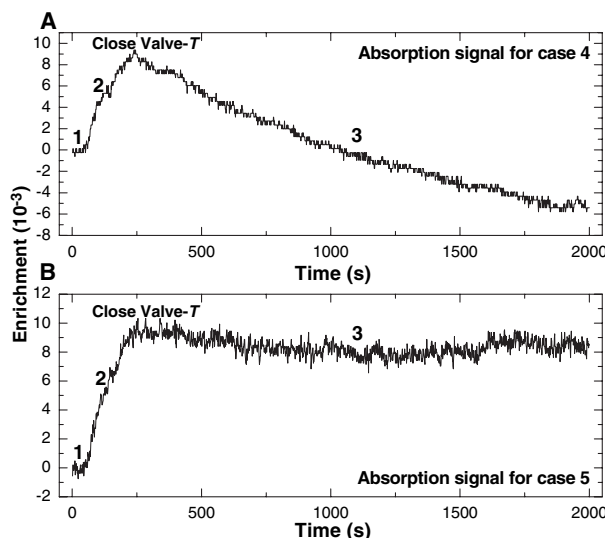


**Fig. 2.** Recorded differential absorption signals at lock-in time constant of 0.3 s using probe  $\text{CO}_2$  laser lines of (A) 10R22 at a pressure of 0.98 torr and (B) 10R28 at a pressure of 1.02 torr. The enrichments are 0.91% ( $\pm 0.05\%$ ) and 0.89% ( $\pm 0.05\%$ ) at the end of the second period of (A) and (B), respectively. The spin conversion rates observed in the third periods of (A) and (B) are  $7.55 (\pm 0.04) \times 10^{-4} \text{ s}^{-1}$  and  $5 (\pm 5) \times 10^{-5} \text{ s}^{-1}$ , respectively.

observe the initial degree of isomer depletion or enrichment. At an ethylene pressure of 1 torr, the probe was tuned through five absorption lines belonging to one of the species  $B_{2u}$ ,  $B_{3u}$ , or  $A_g$  (cases 1 to 5 in the seventh column of Table 2 together with the corresponding absorption coefficients in the sixth column) (18). The depletion of the  $B_{2u}$  species was about 3%, with 1% or less enrichment of the other three isomers.

The equilibration kinetics of the  $B_{2u}$ -depleted sample were measured as follows:

For the first 1-min period, the separation laser was blocked and the valve was kept open to record the zero baseline of the differential signal in the first period. Then, in the second period, the separation laser was unblocked and its beam was introduced into the separation cell for 3 min to generate the nonequilibrium distribution in the test cell. Then the valve was closed, and the decay curves due to isomeric conversion were monitored during the third period. Typical signals are shown for probing  $B_{2u}$  (Fig. 1),  $B_{3u}$  (Fig. 2A) and  $A_g$  (Fig. 2B)

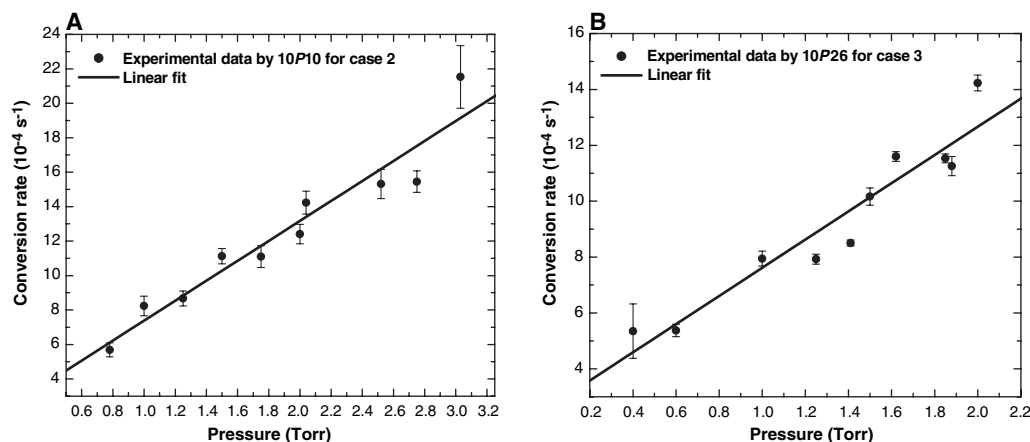


**Fig. 3.** Observed conversion rates as a function of pressure for probing (A) the  $B_{2u}$  species by the 10P10 line and (B) the  $B_{3u}$  species by the 10P26 line of probe  $\text{CO}_2$  laser.

populations. Very similar signals were also observed for alternative  $B_{2u}$  and  $B_{3u}$  probe resonances (cases 2 and 3 in Table 2). We tried to monitor the  $B_{1g}$  population dynamics but were not successful because the line intensity of the resonant  $26_{10,16} \leftarrow 27_{9,18}$  transition was too weak. The signals in the third period show the relaxation due to the conversion among spin isomers. A model function  $A \exp(-\gamma t) + B$  (where  $A$  is the integrated intensity,  $\gamma$  is the observed conversion rate constant, and  $B$  is the baseline offset) was fitted to the decay data of Fig. 1 to give the solid smooth curve shown with a rate constant  $\gamma = 8.09 (\pm 0.10) \times 10^{-4} \text{ s}^{-1}$ .

The data clearly show that the concentration of the  $A_g$  species is almost constant in time, whereas monoexponential kinetics are observed for recovery of the depleted  $B_{2u}$  population and decay of the enriched  $B_{3u}$  population. Furthermore, the  $B_{2u}$  signal does not return to the original zero-difference baseline, and the  $B_{3u}$  signal overshoots the baseline and asymptotically approaches a new equilibrium level. These general phenomena can be qualitatively explained using Curl's theory of state mixing (19). We assume that conversion of nuclear spin isomers of  $\text{C}_2\text{H}_4$  is allowed between the  $B_{2u}$  and  $B_{3u}$  isomers, and between the  $A_g$  and  $B_{1g}$  isomers, but forbidden between species of opposite inversion symmetry. Specifically, molecular "doorway" states are posited, between either  $B_{2u}$  and  $B_{3u}$  or  $A_g$  and  $B_{1g}$ , that are so close in energy that the weak intramolecular nuclear spin-rotation and spin-spin interactions of  $\text{C}_2\text{H}_4$  can induce mixing between them. This mixing is interrupted by collisions, which promote interconversion between either the  $B_{2u}$  and  $B_{3u}$  or the  $A_g$  and  $B_{1g}$  states, through the quantum relaxation process proposed by Chapovsky for *ortho*- and *para*- $\text{CH}_3\text{F}$  (20). Therefore, the time rate of change of the number density of one species is determined by the net number of doorway transitions within species of like inversion symmetry. The concentrations of the  $B_{2u}$  and  $B_{3u}$  species relax exponentially toward a common depleted

equilibrium level, whereas those of the  $A_g$  and  $B_{1g}$  species retain their initial enriched level with no large relaxation. Net population is thus transferred from the  $B_{3u}$  to the  $B_{2u}$  state (reflected in the absorption signal of the  $B_{2u}$  population not reaching the zero-difference baseline, and the  $B_{3u}$  signal passing the baseline).

From the near-constancy of the signal in the third period of Fig. 2B, it appears that spin isomer conversion between states of opposite inversion symmetry is negligible, as is the impact of molecular collisions with the cell wall over the 30-min time range studied. However, over a longer time frame, it is speculated that these factors could cause eventual reequilibrium of the isomer populations to the initial thermal ratios (zero-difference baseline).

The theory of quantum relaxation in *ortho-para* conversion (20) predicts that, at low pressure, the spin conversion rate should vary linearly with the total gas concentration  $p$ . Thus, the observed first-order rate constant is  $\gamma = kp + \gamma_0$ , and varying the pressure allows extraction of the bimolecular rate constant  $k$ . So far, this behavior has been observed for  $\text{CH}_3\text{F}$  (6, 7) and  $^{13}\text{C}^{12}\text{CH}_4$  (8). For  $\text{C}_2\text{H}_4$ , we measured more than 100 conversion tracks at different pressures and observation times, probing at each of the four  $B_{2u}$  and  $B_{3u}$  resonances (Table 2, cases 1 to 4). The mean values of  $\gamma$  are plotted in Fig. 3 as a function of pressure. The data fit reasonably well to a linear pressure dependence. Rate constants from the fits for each probe wavelength agree well within the experimental errors (Table 2) and give an average of  $5.5 (\pm 0.8) \times 10^{-4} \text{ s}^{-1} \text{ torr}^{-1}$ .

Thus, our spin conversion observations for  $\text{C}_2\text{H}_4$  are well accounted for by the model of quantum relaxation. The results provide evidence of the weak intramolecular hyperfine interactions in  $\text{C}_2\text{H}_4$  and suggest that the conversion mechanism among nuclear spin isomers of polyatomic molecules in general is quantum relaxation with conserved inversion symmetry.

## References and Notes

- L. D. Landau, E. M. Lifshitz, *Quantum Mechanics* (Pergamon, Oxford, ed. 3, 1981).
- A. Farkas, *Orthohydrogen, Parahydrogen, and Heavy Hydrogen* (Cambridge Univ. Press, London, 1935).
- H. Kawakita *et al.*, *Science* **294**, 1089 (2001).
- J. E. Dickens, W. M. Irvine, *Astrophys. J.* **518**, 733 (1999).
- N. Dello Russo *et al.*, *Astrophys. J.* **621**, 537 (2005).
- P. L. Chapovsky, *JETP* **70**, 895 (1990).
- B. Nagels, M. Schuurman, P. L. Chapovsky, L. J. F. Hermans, *Phys. Rev. A* **54**, 2050 (1996).
- P. L. Chapovsky, J. Cosléou, F. Herlemont, M. Khelkhal, J. Legrand, *Chem. Phys. Lett.* **322**, 424 (2000).
- G. Peters, B. Schramm, *Chem. Phys. Lett.* **302**, 181 (1999).
- P. R. Bunker, P. Jensen, *Molecular Symmetry and Spectroscopy* (NRC Research Press, Ottawa, ed. 2, 1998), pp. 407–409.
- V. I. Tikhonov, A. A. Volkov, *Science* **296**, 2363 (2002).
- F. Kh. Gel'mukhanov, A. M. Shalagin, *JETP Lett.* **29**, 711 (1979).
- In Table 1, the  $A_g$  species corresponds to all four spins aligned, as well as to the case of no net spin. This species corresponds to the symmetric state with respect to the  $180^\circ$  rotations (or interchanges of H nuclei caused by these rotations) about the  $x$ ,  $y$ , and  $z$  axes and belongs to the rotational states with the same symmetry  $[(K_a, K_c) = (\text{even}, \text{even})]$  because of the Pauli principle. The  $B_{1g}$ ,  $B_{2u}$ , and  $B_{3u}$  species correspond to the case for one total spin. The  $B_{1g}$  state is symmetric with respect to the  $180^\circ$  rotation about the  $z$  axis and antisymmetric to the rotations about the  $x$  and  $y$  axes, belonging to the rotational state with the same symmetry  $[(K_a, K_c) = (\text{odd}, \text{even})]$ ; the  $B_{2u}$  and  $B_{3u}$  states are symmetric with respect to the  $180^\circ$  rotations about the  $y$  and  $x$  axes, respectively, and antisymmetric to those about the other two axes ( $x$  and  $z$ ;  $y$  and  $z$ ), respectively, belonging to the rotational states shown in Table 1. The  $A_g$ ,  $B_{3g}$ ,  $B_{2u}$ , and  $B_{1u}$  species of nuclear spin isomers of  $\text{C}_2\text{H}_4$  given by Bunker and Jensen (10) correspond to the  $A_g$ ,  $B_{1g}$ ,  $B_{2u}$ , and  $B_{3u}$  species, respectively, used in this work.
- G. Herzberg, *Molecular Spectra and Molecular Structure. II. Infrared and Raman Spectra of Polyatomic Molecules* (Van Nostrand Reinhold, New York, 1945).
- T. Oka, *J. Mol. Spectrosc.* **48**, 503 (1973).
- See supporting material on Science Online.
- I. Cauuet *et al.*, *J. Mol. Spectrosc.* **139**, 191 (1990).
- In these measurements, the probe laser was locked to the 4.3- $\mu\text{m}$  Lamb-dip fluorescence signal in an external  $\text{CO}_2$  cell via a closed servo feedback loop (27). To shift the probe  $\text{CO}_2$  laser frequency by 100 or 200 MHz, we used one set (for cases 2 to 4) or two sets in tandem (for case 5) of an acousto-optic modulator (IntraAction AGM-1003A1) and an RF modulator driver (GE-10020), respectively.

19. R. F. Curl Jr., J. V. V. Kasper, K. S. Pitzer, *J. Chem. Phys.* **46**, 3220 (1967).  
 20. P. L. Chapovsky, *Phys. Rev. A* **43**, 3624 (1991).  
 21. Z.-D. Sun, F. Matsushima, S. Tsunekawa, K. Takagi, *J. Opt. Soc. Am. B* **17**, 2068 (2000).  
 22. We express sincere thanks to P. L. Chapovsky for valuable guidance when he visited our laboratory. We thank P. L. Chapovsky and R. M. Lees for critical

reading and commenting on the manuscript; T. Oka and J. T. Hougen for helpful discussions; Y. Moriwaki, K. Uehara, and group members for assistance in this work; and the anonymous referees for their insightful comments. Supported by the Japan Society for the Promotion of Science (JSPS) and grant-in-aid P04063 for JSPS Fellows from the Ministry of Education, Science, Sports, and Culture of Japan (Z.-D.S.).

**Supporting Online Material**  
[www.sciencemag.org/cgi/content/full/310/5756/1938/DC1](http://www.sciencemag.org/cgi/content/full/310/5756/1938/DC1)

Materials and Methods  
 Fig. S1

12 September 2005; accepted 27 October 2005  
 10.1126/science.1120037

# Synthesis of Imido Analogs of the Uranyl Ion

Trevor W. Hayton,<sup>1</sup> James M. Boncella,<sup>1\*</sup> Brian L. Scott,<sup>1</sup>  
 Phillip D. Palmer,<sup>1</sup> Enrique R. Batista,<sup>2</sup> P. Jeffrey Hay<sup>2</sup>

Here we describe the synthesis of two imido analogs of the uranyl ion,  $\text{UO}_2^{2+}$ , in which the oxygens are replaced by divalent alkyl or aryl nitrogen groups:  $\text{U}(\text{N}^t\text{Bu})_2\text{I}_2(\text{THF})_2$  (**1**) and  $\text{U}(\text{NPh})_2\text{I}_2(\text{THF})_3$  (**2**) (where  $^t\text{Bu}$  is *tert*-butyl and THF is tetrahydrofuran). Both compounds have been fully characterized by standard analytical techniques, including x-ray crystallography, and the chemical bonding between the metal center and the nitrogen ligands was quantified by using hybrid density functional theory calculations. As expected for a uranyl analog, these complexes exhibit linear N-U-N linkages and very short U-N bonds. In addition, the theoretical calculations show strong involvement of the 5f and 6d electrons in the U-N bonding.

The uranyl ( $\text{UO}_2^{2+}$ ) species is the most common functional unit in the chemistry of U(VI) and has been known for more than 150 years (1). With the advent of nuclear energy and the use of uranium oxide as reactor fuel, the chemistry of the uranyl ion has played an essential role in the processing of uranium ore, nuclear fuel, and waste (2). The linear arrangement of the oxo ligands, extremely short U-O bond lengths, and high thermal and chemical stability reflect some of the unusual properties of this functional group (3). Given the prevalence of uranyl, it is surprising that metal-ligand multiple bonding in the actinides is not better understood. For instance, it is generally agreed that the uranium-oxygen bonds in uranyl involve six U-O interactions; however, the ordering of the frontier orbitals is still being debated (4). Furthermore, recent high-profile reports, such as the synthesis of a molecular uranium nitride (5) and the isolation of an  $\eta^1$ -O-bound uranium- $\text{CO}_2$  complex (6), point to a general deficiency in our knowledge of the chemistry of the f elements relative to the transition metals. The importance of multiple bonding in the actinides and the extent that the f orbitals participate in bonding are still open questions that can be addressed through the synthesis of new classes of compounds.

The imido ligand ( $\text{NR}^{2-}$ ) is isoelectronic with the oxo ligand, and the two groups can

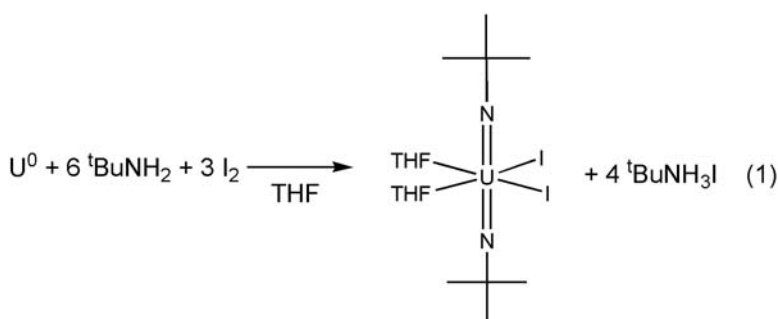
often be interchanged in transition metal complexes. The alkyl or aryl substituent of the imido ligand provides a variable unavailable in oxo chemistry, because changes in the steric and electronic properties of the imido substituent can affect the chemistry of the metal center to which it is bound. The synthesis of the isoelectronic imido analogs of uranyl has therefore been of interest for many years (7). However, direct imido analogs of the uranyl ion have remained elusive despite a great deal of effort toward their synthesis. For instance, Denning

and co-workers were able to isolate the phosphorane-iminato ( $\text{UNPR}_3$ ) and sulfilimine ( $\text{UNSR}_2$ ) substituted analogs of uranyl, which are heteroatom approximations to the imido ligand (7–9). Burns and co-workers were able to synthesize  $\text{Cp}^*\text{U}(\text{NR})_2$  (where R was either Ph or adamantyl and  $\text{Cp}^*$  was  $\text{C}_5\text{Me}_5$ ), but with imido groups in a *cis*-configuration (10, 11). The difficulty in isolating a *trans*-bis(alkyl or aryl imido) complex led Denning to speculate that their isolation was not possible because uranium(VI) is too oxidizing (9).

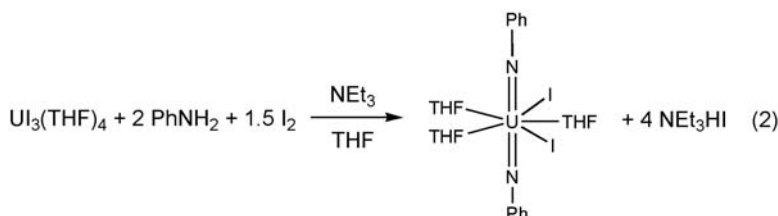
Here we report the synthesis and full characterization of both alkyl and aryl *trans*-bis(imido) analogs of the uranyl ion:  $\text{U}(\text{NR})_2^{2+}$ . By using hybrid density functional theory (DFT), we also compare the calculated and experimental properties of these compounds and analyze the nature of the U-N bonding (12–15).

Reaction of uranium turnings with 3 equivalents of  $\text{I}_2$  and 6 equivalents of *tert*-butylamine in tetrahydrofuran (THF) quickly results in metal dissolution and the formation of an orange solution (Scheme 1). Isolation of a crude orange solid and recrystallization from a toluene/hexanes solution provides crystalline  $\text{U}(\text{N}^t\text{Bu})_2\text{I}_2(\text{THF})_2$  (**1**) in 68% yield (16).

Replacing *tert*-butylamine with aniline in Scheme 1 does not provide any tractable products. However, by starting with well-known



**Scheme 1.**



**Scheme 2.**

<sup>1</sup>Chemistry Division, MS J514, <sup>2</sup>Theoretical Division, MS B268, Los Alamos National Laboratory, Los Alamos, NM 87545, USA.

\*To whom correspondence should be addressed.  
 E-mail: boncella@lanl.gov